

1 ***Supporting Information*** for
2 Atomic-scale visualization and quantification of lithium in lepidolite by
3 AC-TEM-EELS: Implications for pegmatite genesis and advancing
4 lithium extraction techniques

5
6
7 **Contents of this file**

8 Geological background and Figures S1 to S9, and Tables S1 to S3
9

10 **Geological background**

11 The Shaliuquan area is tectonically settled in the Quanji massif (QM), which is
12 located between the Qaidam block and the south Qilian belt, NW China (**Fig. 1 in**
13 **main text**)(Wang et al., 2018, 2020). The Quanji massif is a long and narrow small
14 remnant continental fragment with nearly NW-SE-trending, which is considered to be
15 detached from the Tarim Craton (TC). Therefore, the geological history of the Quanji
16 massif was similar to that of the Tarim craton since the middle Neoproterozoic
17 (Zhang et al., 2012). The basement of Quanji massif is mainly early Paleoproterozoic
18 granitic gneisses and medium- to high-grade metamorphic rocks (Wang et al., 2018;
19 Liao et al., 2018). The overlying strata mainly consists of
20 Mesoproterozoic-Phanerozoic sedimentary rocks (Wang et al., 2019). The
21 metamorphic basement is composed of the early Paleoproterozoic Delingha complex
22 and the amphibolite facies of the Paleoproterozoic Dakendaban Group paragneisses
23 (He et al., 2018; Gong et al., 2019), which is unconformably overlain by the
24 sedimentary strata of the Quanji Group (1.73-1.64 Ga) (Zhang et al., 2017) and Upper
25 Neoproterozoic, Lower Paleozoic to Mesozoic strata (Zhang et al., 2016; Pan et al.,
26 2021).

The Shaliuquan area has experienced many tectonic movements, as a result, many fold and fault structures are developed. The Paleoproterozoic strata in the area leans from the southwest to the northeast and presents as a monocline structure. The secondary folds structures are well developed including the Duantougou anticline, the Amnik mountain syncline, the Xidagou anticline, the Xidagou syncline and the Dongdagou syncline. The metamorphic basement of the Shaliuquan area is mainly composed of the Paleoproterozoic Dakendaban group (NW-SE-trending), which consists of the migmatite formation, the schist formation, and the marble-dolomite-schist formation (Fig. 1 in main text). The pegmatite dike intrudes into the marble-dolomite-schist formation of Paleoproterozoic Dakendaban group through multiple layers, which is the main Li-bearing layer in the area (Fig. S1). The lepidolite pegmatite samples used in this study were collected from the marble-dolomite-schist formation of Paleoproterozoic Dakendaban group in the middle of Shaliuquan area. The lepidolite pegmatite contains 70% of lepidolite, 20% of potassium feldspar and 10% of quartz (Fig. S2). The diameter of lepidolite varies from 0.2 to 2 cm. The edges and cleavages of lepidolite are generally broken (Fig. S3). Potassium feldspar generally presents good crystalline shapes. However, quartz is fragmented, which was formed by the combination of small quartz grains.

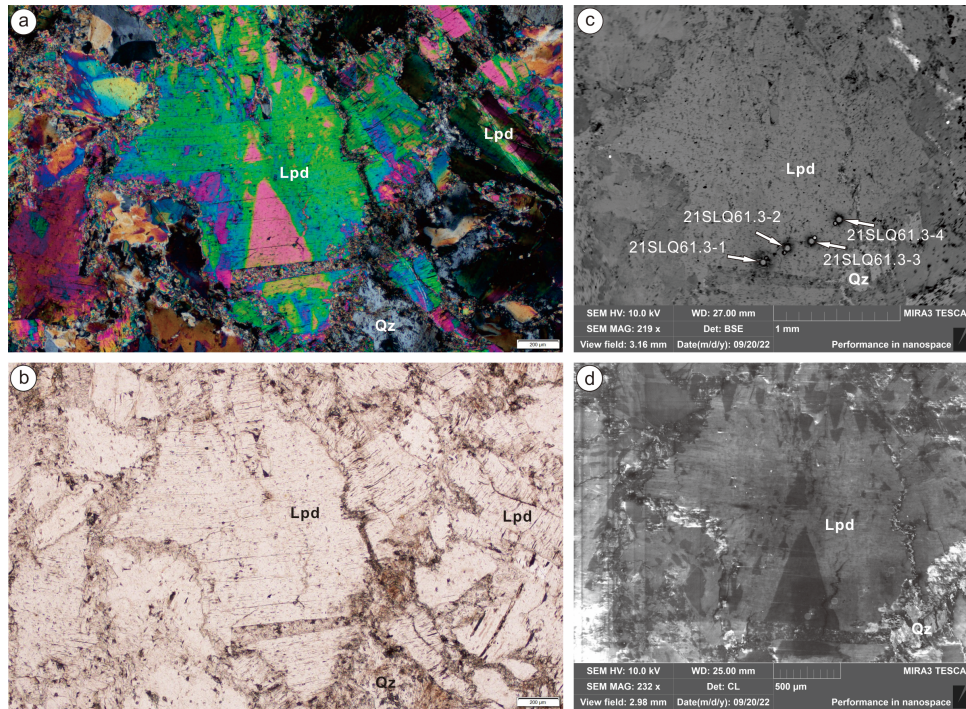


Fig. S3 Micro-photograph of lepidolite grain from sample no. 21SLQ61 for AC-TEM analysis. **(a)** Micro-photograph under cross-polarized light. **(b)** Micro-photograph under transmission light, the markers are the EPMA and LA-ICP-MS analysis positions. **(c)** Back scatter photograph. **(d)** Cathodeluminescence photograph. Lpd: lepidolite. Qz: quartz

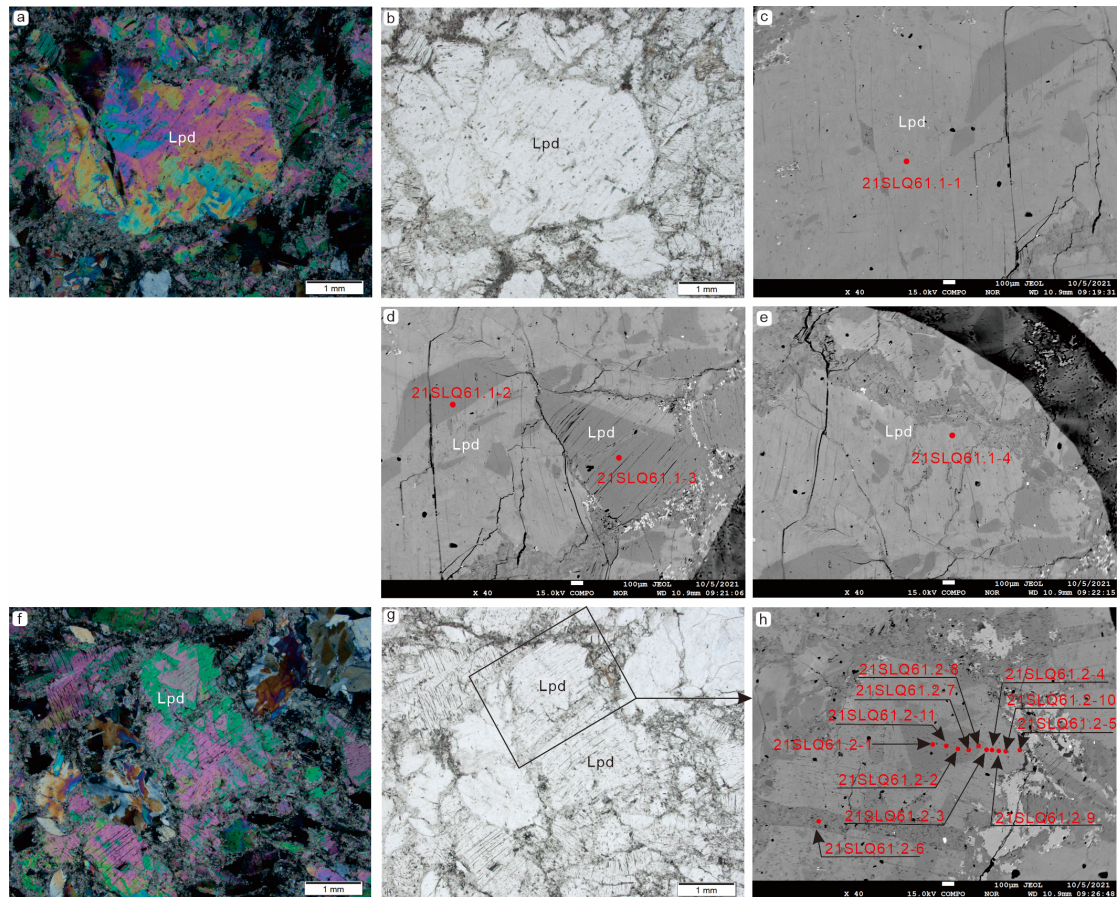


Fig. S4 Micro-photograph of lepidolite grains from sample no. 21SLQ61 for EPMA analysis. **(a, f)** Micro-photograph under cross-polarized light. **(b, g)** Micro-photograph under transmission light. **(c, d, e, h)** Back scatter photographs with the locations for EPMA analysis. Lpd: lepidolite

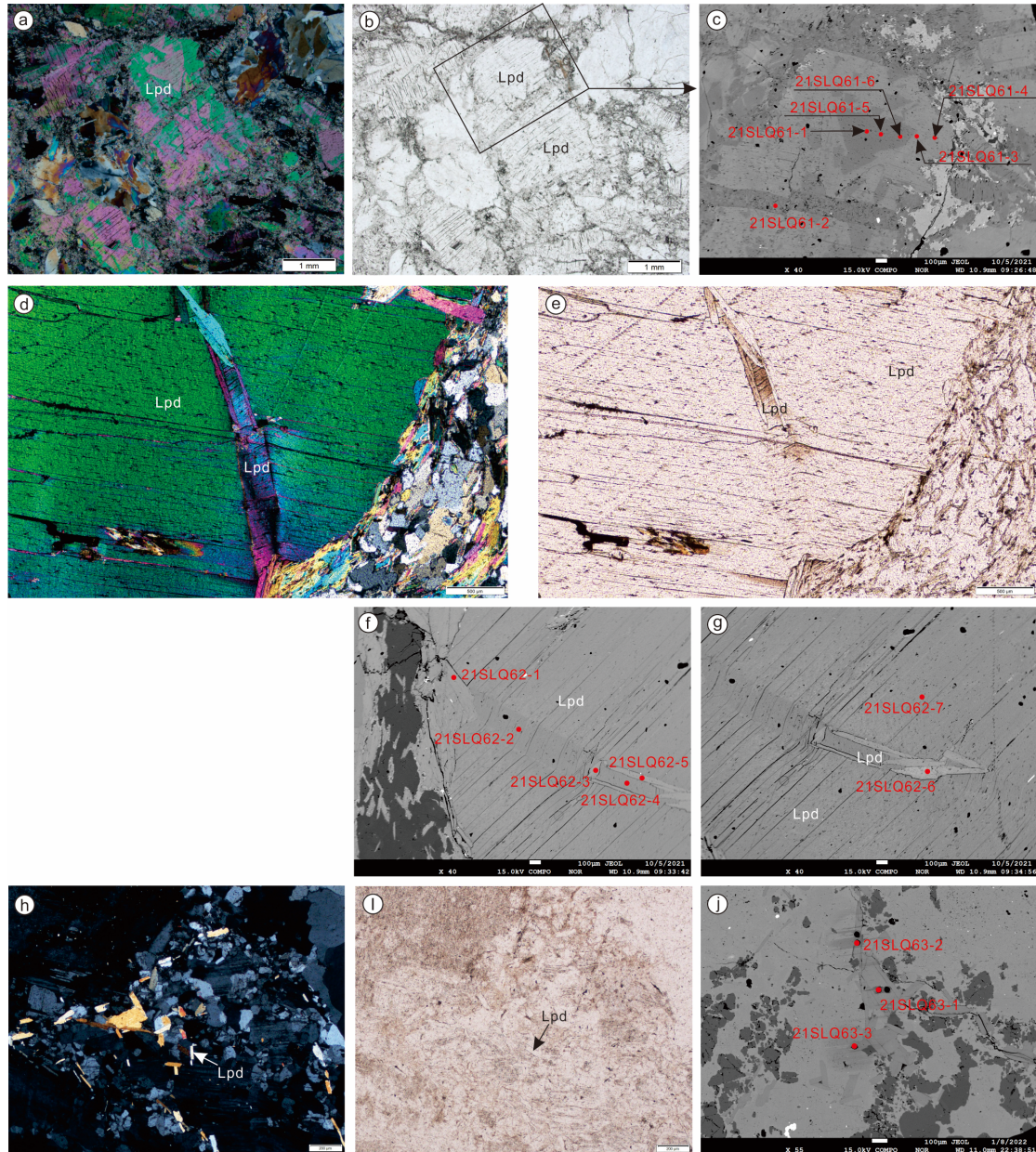


Fig. S5 Micro-photograph of lepidolite grains from sample no. 21SLQ61, 21SLQ62 and 21SLQ63 for LA-ICP-MS analysis. **(a, d, h)** Micro- photograph under cross-polarized light. **(b, e, i)** Micro-photograph under transmission light. **(c, f, g, j)** Back scatter photographs with the locations for LA-ICP-MS analysis. Lpd: lepidolite

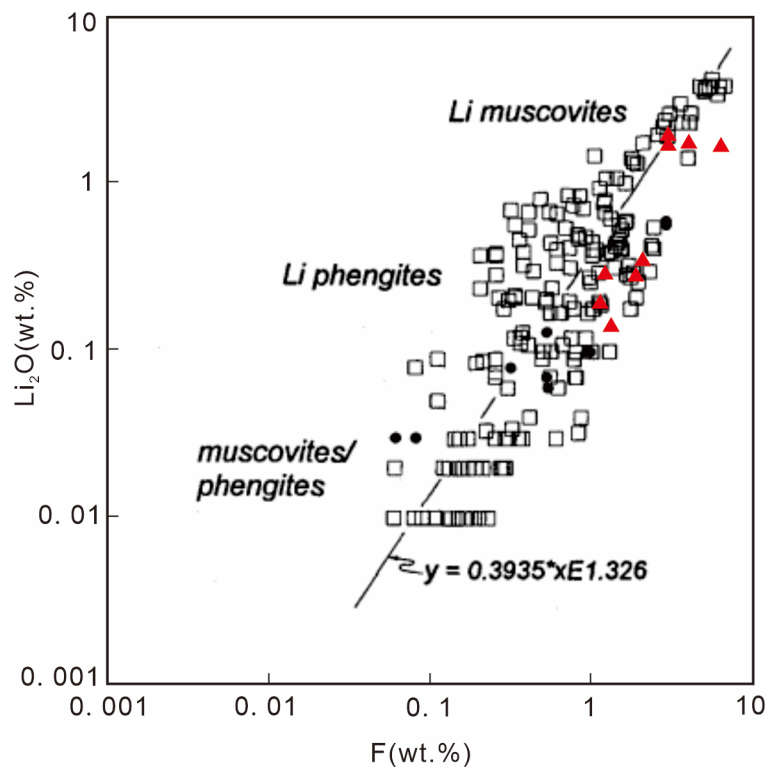


Fig S6 Variation of Li_2O with F (Modified after [Tischendorf et al. 1997](#)), the red data points represent our study's contributions to this correlation.

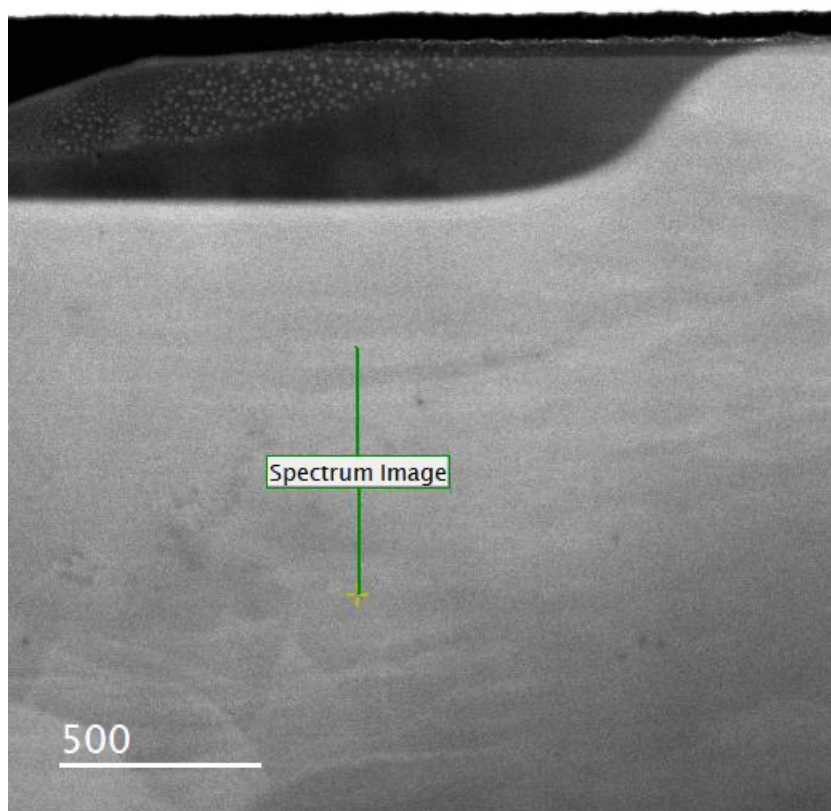


Fig S7 Analysis location of EELS under line-scan mode

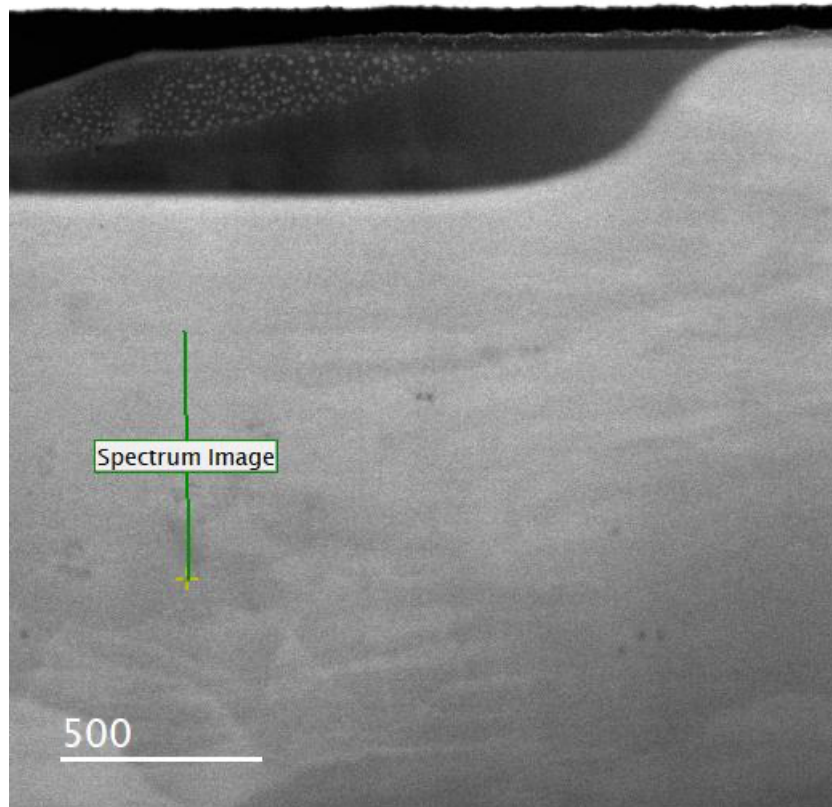


Fig S8 Analysis location of EELS under line-scan mode

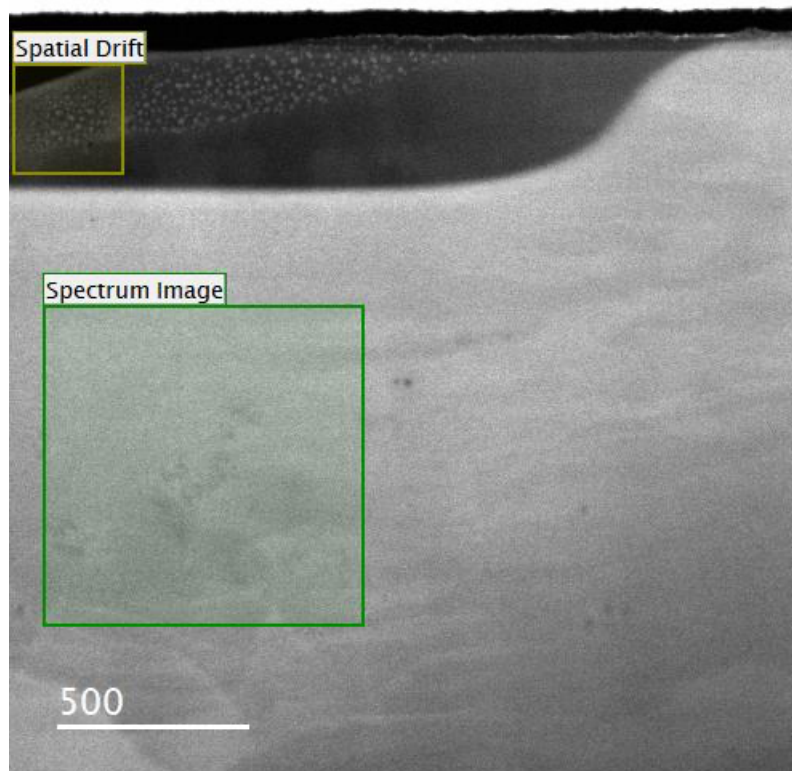
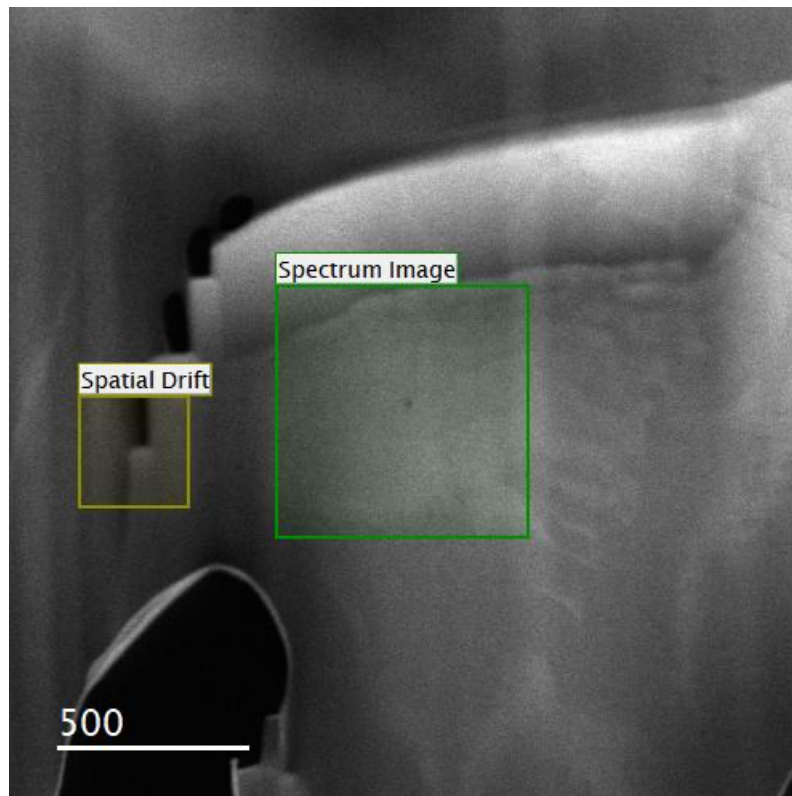


Fig S9 Analysis location of EELS under area-scan mode

90



91

92

Fig S10 Analysis location of EELS under area-scan mode

Table. S1 Electron probe analysis results of lepidolite (wt%)

Analysis no.	SiO ₂	TiO ₂	Al ₂ O ₃	FeO	MnO	MgO	CaO	Na ₂ O	K ₂ O	F	Li ₂ O*	Total*
21SLQ61.3-1	46.263	0.029	37.673	0.179	0.269	\	\	0.657	10.810	2.038	0.949	98.867
21SLQ61.3-2	46.174	\	36.699	0.185	0.293	0.014	0.007	0.544	10.656	1.303	0.546	96.421
21SLQ61.3-3	49.157	\	29.909	0.254	0.627	0.105	\	0.347	10.869	3.232	1.677	96.177
21SLQ61.3-4	50.559	0.022	28.229	0.331	0.853	0.145	0.015	0.276	10.777	3.235	1.679	96.121
21SLQ61.1-1	49.325	\	28.369	0.332	0.949	0.127	0.011	0.252	10.632	5.576	3.292	98.865
21SLQ61.1-2	45.866	0.015	34.869	0.121	0.314	0.002	0.032	0.511	10.189	2.195	1.040	95.154
21SLQ61.1-3	45.924	0.006	35.361	0.141	0.310	0.028	0.038	0.473	10.224	2.258	1.077	95.840
21SLQ61.1-4	49.532	0.007	29.218	0.271	0.557	0.103	0.041	0.235	10.562	5.048	2.911	98.485
21SLQ61.2-1	45.879	\	36.866	0.093	0.237	\	\	0.536	10.453	1.416	0.605	96.085
21SLQ61.2-2	45.374	0.030	37.438	0.087	0.212	\	\	0.528	10.453	1.215	0.501	95.838
21SLQ61.2-3	48.085	0.031	31.487	0.351	0.655	0.107	\	0.250	10.840	4.367	2.433	98.606
21SLQ61.2-4	50.063	\	28.850	0.357	0.857	0.142	0.014	0.258	10.858	5.348	3.126	99.873
21SLQ61.2-5	50.116	\	28.329	0.392	0.898	0.138	\	0.181	10.869	6.099	3.677	100.699
21SLQ61.2-6	45.862	\	36.763	0.093	0.224	\	0.029	0.521	10.182	1.451	0.623	95.748
21SLQ61.2-7	46.268	\	36.154	0.137	0.169	\	0.017	0.469	10.612	1.618	0.713	96.157
21SLQ61.2-8	46.353	\	35.451	0.172	0.336	0.044	\	0.406	10.632	2.240	1.066	96.700
21SLQ61.2-9	49.945	0.041	28.014	0.368	1.053	0.159	\	0.225	10.647	6.950	4.322	101.724
21SLQ61.2-10	49.297	\	28.797	0.306	0.952	0.145	0.012	0.225	10.411	5.860	3.500	99.505
21SLQ61.2-11	45.080	0.04	37.78	0.10	0.16	0.01	0.02	0.41	10.92	0.68	0.246	94.726

* : Li₂O (%) = $0.3935 \times F^{1.326}$ (Tischendorf et al., 1997) ; \ : Below the detection limit.

Table. S2 LA-ICP-MS analysis results of lepidolite (ppm)

No.	Li	Be	B	P	Cl	K	Sc	V	Cr	Co	Ni	Zn	Ga	Ge	Rb	Sr	Y	Zr	Nb	Mo	Sn
21SLQ61.3-1	2732.000	46.400	702.000	\	\	89737.053	\	\	\	\	\	146.900	\	\	6574.000	0.430	\	\	38.500	\	341.300
21SLQ61.3-2	2823.000	46.700	711.000	145.000	\	90226.830	\	\	\	\	\	153.300	\	\	6623.000	0.340	\	\	47.200	\	385.300
21SLQ61.3-3	18700.000	47.800	210.200	106.000	\	92094.622	\	\	\	\	\	461.000	\	\	10640.000		\	\	102.600	\	199.700
21SLQ61.3-4	16540.000	50.600	256.500	72.000	\	89164.263	\	\	6.900	0.320	\	496.000	\	\	9820.000	0.274	\	\	94.100	\	208.700
21SLQ61-1	1353.988	38.577	836.930	217.292	268.723	89258.077	0.723	\	0.758	0.077	1.161	90.156	153.406	7.480	5818.918	0.327	\	0.052	28.524	\	\
21SLQ61-2	2584.535	33.437	757.065	98.480	744.276	92212.674	0.507	\	8.669	0.003	2.536	106.751	153.148	8.530	6181.065	0.287	\	\	35.459	0.178	\
21SLQ61-3	17023.781	53.361	253.711	145.903	497.930	92938.258	0.630	0.006	5.820	\	2.490	399.010	87.939	12.996	9800.180	0.386	0.018	0.235	86.913	0.263	\
21SLQ61-4	16392.354	53.681	278.098	117.133	532.495	91485.460	0.537	0.040	2.601	0.449	\	373.296	78.162	11.310	9228.156	0.226	0.020	0.341	83.188		\
21SLQ61-5	1879.494	36.272	633.481	\	326.109	94312.670	0.452	0.825	\	0.051	3.857	137.600	164.188	10.900	3930.815	2.094	\	0.044	39.874		\
21SLQ61-6	3379.643	34.131	662.582	34.271	775.021	94660.938	0.477	\	3.320	0.161	\	123.574	155.194	15.770	6579.022	0.433	\	0.342	39.207	0.328	\
21SLQ62-1	1515.405	56.337	202.014	\	449.060	96847.030	2.519	0.496	\	0.083	\	265.702	178.454	6.511	3868.098	1.247	0.009	0.102	208.885	0.083	\
21SLQ62-2	900.755	40.484	137.926	113.842	523.266	95956.210	1.716	0.226	4.835		\	212.034	183.801	6.692	3826.391	0.503	0.059	0.519	278.099	\	\
21SLQ62-3	1785.619	88.377	403.285	\	387.622	97142.369	1.897	1.666	1.417	0.101	1.024	371.831	141.805	7.724	4123.551	1.051	\	0.223	188.075	\	\
21SLQ62-4	798.401	49.071	146.905	114.639	618.768	96257.273	1.703	0.036	\	0.021	1.431	188.090	175.118	5.674	3751.294	0.664	0.010	0.643	291.268	\	\
21SLQ62-5	1550.932	64.981	288.577	39.851	474.749	96967.715	2.619	1.129	\	0.205	\	361.711	176.855	5.468	3993.403	1.135	0.009	0.143	239.797	0.068	\
21SLQ62-6	1887.456	76.851	409.478	17.261	352.125	96447.253	2.050	1.845	\	0.250	0.329	365.222	145.807	5.727	4104.673	1.084	0.018	0.182	210.076	\	\
21SLQ62-7	483.276	25.316	120.837	105.270	441.887	93277.575	2.305	0.082	0.403	0.143	1.910	424.871	185.527	3.370	3759.689	0.032	\	0.488	294.682	0.213	\
21SLQ63-1	2033.000	95.500	246.000	\	\	92152.731	1.490	2.010	36.000	1.850	2.200	296.000	\	\	3712.000	4.300	\	\	193.000	\	227.900
21SLQ63-2	1931.000	82.600	227.900	\	\	90567.183	1.700	1.770	\	1.350	\	298.000	\	\	3726.000	1.010	\	\	201.300	\	191.100
21SLQ63-3	1767.000	77.000	180.000	\	\	92874.944	1.960	2.490	14.000	1.780	3.100	234.000	\	\	3450.000	2.700	\	\	175.000	\	237.000

Continue to Table 2

No.	Cs	Ba	La	Ce	Pr	Nd	Sm	Eu	Gd	Tb	Dy	Ho	Er	Tm	Yb	Lu	Ta	Pb	Th	U
21SLQ61.3-1	1039.000	\	0.170	\	\	\	\	\	\	\	\	\	\	\	\	\	46.130	3.440	\	\
21SLQ61.3-2	1106.000	\	0.129	\	\	\	\	\	\	\	\	\	\	\	\	\	55.500	4.070	\	\
21SLQ61.3-3	2936.000	\	\	\	\	\	\	\	\	\	\	\	\	\	\	\	154.100	2.440	\	\
21SLQ61.3-4	2440.000	\	\	\	\	\	\	\	\	\	\	\	\	\	\	\	144.200	2.210	\	\
21SLQ61-1	686.636	3.831	0.282	0.123	0.016	0.097	0.222	\	\	0.016	\	\	0.048	0.015	\	\	32.944	5.120	\	0.036
21SLQ61-2	876.138	8.653	0.286	0.104	\	0.099	0.024	\	\	\	\	\	0.049	\	\	\	46.677	3.735	\	0.036
21SLQ61-3	2127.523	2.738	0.671	0.215	\	0.073	\	\	\	0.012	\	\	\	0.011	0.108	0.024	152.410	1.855	0.030	0.013

21SLQ61-4	2281.878	4.782	0.313	0.083	\	\	\	\	\	\	0.011	0.013	\	\	\	0.027	164.002	2.521	\	\
21SLQ61-5	145.908	81.490	0.827	0.348	0.040	\	\	0.050	0.093	\	\	0.014	\	\	\	0.014	8.274	4.241	0.034	\
21SLQ61-6	969.502	0.879	0.342	0.171	0.015	0.091	\	0.028	\	0.030	0.060	\	\	\	\	\	51.523	3.673	\	0.033
21SLQ62-1	347.218	153.255	0.166	0.072	\	\	0.043	\	\	0.006	\	\	0.037	\	\	\	20.891	4.213	\	\
21SLQ62-2	136.941	57.010	0.229	0.059	\	0.009	0.046	0.025	\	0.020	0.027	0.014	\	0.006	0.036	\	37.993	2.702	\	0.002
21SLQ62-3	437.608	227.908	0.107	0.033	\	\	0.043	\	\	0.013	\	0.006	0.037	\	0.028	0.013	25.439	4.778	0.008	\
21SLQ62-4	103.106	16.726	0.504	0.234	\	\	\	0.025	\	\	0.054	\	\	\	\	\	38.936	3.536	\	0.015
21SLQ62-5	367.140	158.953	0.174	0.095	\	0.038	0.087	0.023	\	\	\	\	\	0.018	0.056	0.006	29.811	4.970	\	\
21SLQ62-6	426.891	221.129	0.016	0.002	\	\	\	0.046	\	\	0.025	0.006	0.037	0.012	0.055	0.013	27.268	4.760	\	0.007
21SLQ62-7	98.983	1.380	0.036	0.051	\	0.008	\	0.024	0.044	\	0.026	\	\	\	\	0.013	39.306	2.175	\	0.014
21SLQ63-1	377.900	\	0.140	0.640	\	\	\	\	0.300	\	0.300	\	\	\	\	\	65.300	6.240	\	\
21SLQ63-2	444.000	\	\	\	\	\	\	\	\	\	\	\	\	\	\	\	41.100	5.310	\	\
21SLQ63-3	320.000	\	\	\	\	\	\	\	\	\	\	\	\	\	\	\	52.800	5.100	\	\

\ : Below the detection limit.

Table. S3 Li content of lepidolite using in Figure 2e obtained by EMP and LA-ICP-MS

Method	Sample no.	Li (wt%)	Li ₂ O(wt%)
EMP	21SLQ61.3-1	0.4409	0.949 ^a
EMP	21SLQ61.3-2	0.2537	0.546 ^a
EMP	21SLQ61.3-3	0.7791	1.677 ^a
EMP	21SLQ61.3-4	0.7800	1.679 ^a
EMP	21SLQ61.2-6	0.2811	0.623 ^a
EMP	21SLQ61.2-1	0.2894	0.605 ^a
EMP	21SLQ62.1-11	0.1143	0.246 ^a
EMP	21SLQ62.1-7	0.3312	0.713 ^a
EMP	21SLQ62.1-3	1.1303	2.433 ^a
EMP	21SLQ62.1-10	1.6260	3.500 ^a
LA-ICP-MS	21SLQ61.3-1	0.2732	0.59 ^b
LA-ICP-MS	21SLQ61.3-2	0.2823	0.61 ^b
LA-ICP-MS	21SLQ61.3-3	0.1870	4.03 ^b

LA-ICP-MS	21SLQ61.3-4	0.1654	3.56 ^b
LA-ICP-MS	21SLQ61-2	0.2585	0.56 ^b
LA-ICP-MS	21SLQ61-1	0.1354	0.29 ^b
LA-ICP-MS	21SLQ61-5	0.1880	0.40 ^b
LA-ICP-MS	21SLQ61-6	0.3380	0.73 ^b
LA-ICP-MS	21SLQ61-3	1.7024	3.66 ^b
LA-ICP-MS	21SLQ61-4	1.6392	3.53 ^b

^a : $\text{Li}_2\text{O (wt\%)} = 0.3935 \times F^{1.326}$ (Tischendorf et al., 1997); ^b : $\text{Li}_2\text{O}_{(\text{wt\%})} = (\text{Li}_{(\text{wt\%})} \times M(\text{Li}_2\text{O})) / (M_{\text{Li}} \times 2)$, $M(\text{Li}_2\text{O}) = 29.88$, $M_{\text{Li}} = 6.941$

Table. S4 Differences between lepidolite compositions of FIB sections in Figure 2h and 2g obtained by AC-TEM-EELS, EMP and LA-ICP-MS

Method	Sample no.	Li	Li ₂ O(wt%)	K (ppm)	K ₂ O(wt%)
EMP	21SLQ61.3-1	0.44%	0.949 ^a	\	10.810
EMP	21SLQ61.3-2	0.25%	0.546 ^a	\	10.656
EMP	21SLQ61.3-3	0.78%	1.677 ^a	\	10.869
EMP	21SLQ61.3-4	0.78%	1.679 ^a	\	10.777
LA-ICP-MS	21SLQ61.3-1	2732 ppm	0.59 ^b	89737.053	\
LA-ICP-MS	21SLQ61.3-2	2823 ppm	0.61 ^b	90226.830	\
LA-ICP-MS	21SLQ61.3-3	18700 ppm	3.56 ^b	92094.622	\
LA-ICP-MS	21SLQ61.3-4	16540 ppm	4.03 ^b	89164.263	\
AC-TEM-EELS	No.1 from 21SLQ61.3-2	1.20 at%	0.88 ^c	\	10.01
AC-TEM-EELS	No.3 from 21SLQ61.3-4	2.66 at%	1.94 ^c	\	10.16

^a : $\text{Li}_2\text{O (wt\%)} = 0.3935 \times F^{1.326}$ (Tischendorf et al., 1997); ^{b,c} : $\text{Li}_2\text{O} = (\text{Li}_{(\text{wt\%})} \times M(\text{Li}_2\text{O})) / (M_{\text{Li}} \times 2)$, $M(\text{Li}_2\text{O}) = 29.88$, $M_{\text{Li}} = 6.941$; the calculation of $\text{Li}_{(\text{wt\%})}$ from $\text{Li}_{(\text{at\%})}$ was using the software programed by A.Murakami.

Reference

- Gong S.L., He C., Wang X.C., Chen N.S., & Kusky T. (2019). No plate tectonic shutdown in the early Paleoproterozoic: constraints from the ca. 2.4 Ga granitoids in the Quanji Massif, NW China. *J. Asian Earth Sci.* 172, 221-242.
- He C., Gong S.L., Wang L., Chen N.S., Santosh M., & Wang Q.Y. (2018). Protracted postcollisional magmatism during plate subduction shutdown in early Paleoproterozoic: insights from post-collisional granitoid suite in NW China. *Gondwana Res.* 55, 92-111.
- Liao F., Wang Q.Y., Chen N.S., Santosh M., Xu Y.X., & Mustafa H.A. (2018). Geochemistry and geochronology of the ~0.82 Ga high-Mg gabbroic dykes from the Quanji Massif, southeast Tarim Block, NW China: implications for the Rodinia supercontinent assembly. *J. Asian Earth Sci.* 157, 3-21.
- Pan T., Ding Q.F., Zhou X., Li S.P., Han J., & Cheng L. (2021). ColumbiteTantalite Group Mineral U-Pb Geochronology of Chaqiabeishan Li-Rich Granitic Pegmatites in the Quanji Massif, NW China: Implications for the Genesis and Emplacement Ages of Pegmatites. *Front. Earth Sci.* 8, 606951.
- Tischendorf, G., Gottesmann, B., Hans-Jürgen, Frster., & Trurnbull, R.B., (1997). On Li-bearing micas: Estimating Li from electron microprobe analyses and an improved diagram for graphical representation. *Mineralogical Magazine* 61, 809-834.
- Wang B.Z., Han J., Xie X.L., Chen J., Wang T., Xue W.W., Bai Z.H., & Li S.P., (2020). Discovery of the indosinian (Beryl-bearing) spodumene pegmatitic dike swarm in the chakaibeishan area in the northeastern margin of the Tibetan plateau: implications for Li-Be mineralization. *Geotect. Et Metallogenia.* 44, 69-79. (in Chinese with English abstract)
- Wang L., Johnston S.T., & Chen N.S., (2019). New insights into the Precambrian tectonic evolution and continental affinity of the Qilian block: evidence from geochronology and geochemistry of metasupracrustal rocks in the North Wulan terrane. *Geol. Soc. Am. Bull.* 131, 1723–1743.
- Wang Q.Y., Dong Y.J., Pan Y.M., Liao F.X., & Guo X.W., (2018). Early paleozoic

granulite-facies metamorphism and magmatism in the northern wulan terrane of the quanji massif: implications for the evolution of the Proto-Tethys ocean in northwestern China. *J. Earth Sci.* 29, 1081-1101.

Zhang L., BA J., Chen N.S., Wang Q.Y., Liao F.X., & Li X.Y., (2012). U-Pb age spectra and trace elements of detrital zircon from quanji group: implications for thermal events and early evolution in the basement. *J. Earth Sci.* 37, 28-42.

Zhang H.J., Wang X.L., Wang X., & Zhou H.R., (2016). U-Pb zircon ages of tuff from the Hongzaoshan Formation, Quanji Group, in the north margin of Qaidam Basin, NW China, and their geological significances. *Earth Sci. Front.* 23, 202-218.

Zhang J.X., Yu S.Y., & Mattinson C.G., (2017). Early paleozoic polyphase metamorphism in northern Tibet, China. *Gondwana Res.* 41, 267-289.